P-ISSN 2586-9000
E-ISSN 2586-9027
Homepage : https://tci-thaijo.org/index.php/SciTechAsia Science & Technology Asia
Vol.25 No.1 January - March 2020 Page: [19-30]
Original research article

MHD Fluid Flow with Cross-Diffusion Effects through Channel Using Optimal Homotopy Analysis Method

Khushbu Bhaskar[1,*], Kalpna Sharma[1], Sumit Gupta[2], Ruchika Mehta[1]

[1]*Department of Mathematics & Statistics, Manipal University Jaipur, Jaipur-303007, India*
[2]*Department of Mathematics, Swami Keshvanand Institute of Technology, Management and Gramothan, Jaipur-302017, India*

Received 30 August 2019; Received in revised form 13 January 2020
Accepted 14 January 2020; Available online 26 March 2020

ABSTRACT

The intention of the present study is to investigate the cross-diffusion effect on MHD fluid flow passing through a vertical channel. Navier slip boundary conditions are applied by assuming that the channel is filled with a porous medium. The effect of considered parameters is also studied on heat as well as on mass transfer. With the help of an optimal homotopic procedure, the transformed governing equations are evaluated. The quantitative estimates are contributed through graphs and physical quantities are presented through a table.

Keywords: Dufour effect; MHD; Navier slip; OHAM; Soret effect

1. Introduction

A porous medium is a substance which has pores. Numerous natural substances such as rocks, soil, wood, cork can be considered as porous media. The porous media is used in various science, engineering and biomedical applications such as soil and rock mechanics, petroleum technology, dying process, material science, human lungs, small bold capillaries, etc. Porous medium describes the two prompt properties, namely porosity and permeability. Porosity evaluates the amount of fluid tackled by the material while permeability measures quantitatively the ability of the porous medium to permit fluid flow. Magnetohydrodynamic fluid flow through porous medium has many significant roles in pure science, engineering, technological, and biomedical fields such as MHD power generators, MHD accelerators, blood flow measurements, electrolytes, ionized gases,

***Corresponding author:** bhaskarkhushbu@gmail.com **doi:** 10.14456/scitechasia.2020.3

traveling waves tubes, metal-working processes, propulsion units, control fusion research, etc. In boundary layer flow problems, MHD controls the force and heat exchanged by the surface. Srinivas and Muthuraj [1] debilitated the homotopy analysis method to find an approximate solution for the MHD flow of viscous incompressible fluid with thermal radiation and porosity effects. Raftari and Vajravelu [2] investigated the magnetohydrodynamic viscoelastic fluid characteristic through a wall. Heat transfer for micropolar fluid embedded in a porous medium was explored by Xinhui et al. [3]. The homotopy perturbation method used to discuss the influence of thermal radiation, chemical reaction and inclined magnetic field over a vertical channel was scrutinized by Kothandapani and Prakash [4]. Ellahi et al. [5] evaluated magnetohydrodynamic flow of Power-Eyring fluid through slip conditions. MHD flow over an exponentially stretching surface embedded by porous medium and thermal radiation was elucidated by Sharma and Gupta [6]. Kumar et al. [7] discussed entropy generation of magnetohydrodynamic flow over a rotating channel with the porosity effect. Oscillatory flow with the uniform magnetic field and viscous dissipation over a channel was reviewed by Selvi and Muthuraj [8]. Farooq et al. [9] investigated the transverse magnetic field variation over a non-uniform channel with slip condition. Kumar et al. [10] examined the effects of a constant heat source on fractional exothermic reactions model with exponential, power and Mittag-Leffler laws in a porous medium. The boundary layer flow for viscous fluid over a flat plate was evaluated by Sushila et al. [11].

In recent years, the analysis of Dufour and Soret effects has had great significance and attracted various scientists and researchers due to its applications in engineering, industry and geosciences such as hydrology, petrology, turbine blades, foam combustion, gas-particle trajectories, etc. It is observed that the flux of heat caused due to the gradient of composition is known as diffusion-thermo or Dufour effect. The mass flux that occurs due to temperature gradient is called thermal-diffusion or Soret effect. In mass and heat transfer processes, cross-diffusion effects are often neglected due to their small order of magnitude as compared with Fick's and Fourier's law. Numerical investigation of non-Newtonian fluid flow over a vertical channel with Hall effect and Soret & Dufour effects was reported by Reddy et al. [12]. Mahmoud and Megahed [13] reviewed the thermal-diffusion and diffusion-thermo effects on fluid flow with mixed radiation and thermal radiation properties. Kaladhar and Komuraiah [14] published their work on fluid flow with the effect of Soret, Dufour, and Navier slip conditions. Ahmed et al. [15] presented an analysis of the Dufour and Soret effects on MHD free convective viscous fluid flow through a channel.

A mathematical formulation of fluid flow problems can be derived from Navier-Stokes equations which are non-linear differential equations in nature. Solutions of these differential equations can be obtained by numerical or analytical methods such as homotopy perturbation method (HPM), homotopy analysis method (HAM), homotopy analysis transform method (HATM), Adomian decomposition scheme, variational iteration approach, Laplace decomposition scheme, Runge-Kutta method, shooting method, etc. Goswami et al. [16, 17] worked on HPSTM to find the exact solution of regularized long wave equations in cold plasma. Kumar et al. [18] studied the HATM to determine the solution of nonlin-

ear wave-like differential equations. Singh et al. [19] investigated the Jeffery-Hamel fluid flow through non-parallel walls using the homotopy analysis transform method. In the present problem, we are using the OHAM method. This method was first initiated by Liao [20, 21]. In the present problem, Mathematica based BVPh 2.0 is used to elucidate the solution of transformed nonlinear coupled ordinary differential equations. Many scientists and researchers have worked on the problems related to channels because they have substantial utilization in science and engineering. Fluid low over a deformable channel with the presence of heat transfer has been examined by Asghar et al. [22]. The impact of slip boundary on the non-Newtonian fluid through a channel was studied by Ellahi [23]. Ng [24] discussed the fluid flow with slip boundary over a permeable channel. Sharma and Gupta [25] discussed the magnetohydrodynamic flow over an inclined surface bounded by the convective boundaries. Terekhov et al. [26] numerically investigated the heat transfer properties over vertical isothermal plates. Joule heating and thermal radiation impact on MHD flow of nanofluid over a vertical channel was studied by Srinivasacharya and Shafeeurrahman [27].

The main theme of the current research is to elucidate the effects of cross-diffusion and chemical reaction on the MHD fluid flow by assuming both heat and mass transfer characteristics through an upstanding channel that is filled with porous medium and Navier slip conditions. The transformed system of equations is then evaluated by the optimal homotopy analysis method (OHAM).

2. Mathematical Modelling

Consider an incompressible 2-D electrically conducting flow through an uplifting channel. Heat and mass transfer characteristics are considered through the Fourier's and Fick's Law of thermodynamics. Flow is induced by the Navier slip conditions by implementing on the boundary of the governing flow problem. A constant magnetic field is implemented

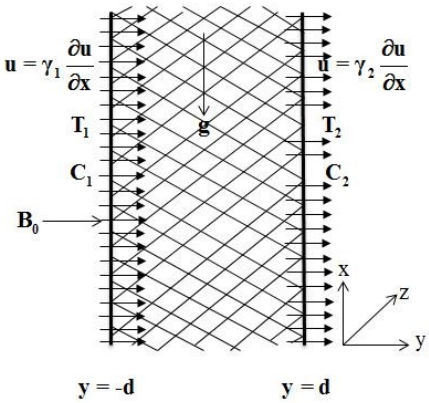

Fig. 1. Physical model.

normal to the plates; moreover, the induced magnetic field is assumed to be negligible. The representation of the problem is shown in Fig. 1. Using the above-mentioned assumption the governing equations are:

$$v_y = 0 \Rightarrow v = v_0 = \text{constant}; \qquad (2.1)$$

$$v_0\rho\frac{\partial u}{\partial y} = \rho g\{\beta_T(T - T_1) + \beta_C(C - C_1)\} + \mu\frac{\partial^2 u}{\partial y^2} - \sigma B_0^2 u - \frac{\mu}{\kappa}u; \qquad (2.2)$$

$$\rho C_p v_0\frac{\partial T}{\partial y} = K_f\frac{\partial^2 T}{\partial y^2} + \mu\left(\frac{\partial u}{\partial y}\right)^2 + \frac{\rho D K_T}{C_s}\frac{\partial^2 C}{\partial y^2} + \frac{\mu}{\kappa}u^2; \qquad (2.3)$$

$$v_0\frac{\partial C}{\partial y} = D\frac{\partial^2 C}{\partial y^2} + \frac{DK_T}{T_m}\frac{\partial^2 T}{\partial y^2} - K_1(C - C_1); \tag{2.4}$$

with the boundary conditions

$$\begin{aligned} u &= \gamma_1\frac{\partial u}{\partial y}, \quad T = T_1, \quad C = C_1 \quad \text{at } y = -d, \\ u &= \gamma_2\frac{\partial u}{\partial y}, \quad T = T_2, \quad C = C_2 \quad \text{at } y = d. \end{aligned} \tag{2.5}$$

Non-dimensional variables are introduced as

$$\eta = \frac{y}{d}, u = u_o f, \theta = \frac{T - T_1}{T_2 - T_1}, \varphi = \frac{C - C_1}{C_2 - C_1}. \tag{2.6}$$

Using these non-dimensional parameters in equations (2.2)-(2.5), we get the governing dimensionless equations as

$$f'' - Rf' + \lambda(\theta + \beta\varphi) - \left(M^2 + K_p\right) f = 0; \tag{2.7}$$

$$\theta'' - R\,\mathrm{Pr}\,\theta' + \mathrm{Pr}\,Ec\,(f')^2 + \mathrm{Pr}\,D_f\varphi'' + \mathrm{Pr}\,EcK_p f^2 = 0; \tag{2.8}$$

$$\varphi'' - RSc\varphi' + ScSr\theta'' - KSc\varphi = 0; \tag{2.9}$$

with

$$\begin{aligned} \eta = -1: \ & f - \beta_1 f' = \theta = \varphi = 0; \\ \eta = 1: \ & f - \beta_2 f' = 0, \theta = \varphi = 1. \end{aligned} \tag{2.10}$$

Where the prime denotes differentiation with respect to η, $R = \frac{\rho v_0 d}{\mu}$ represents suction/injection parameter, $\mathrm{Re} = \frac{\rho u_0 d}{\mu}$ indicates Reynolds number, $Gr_T = \frac{g\beta_T (T_2 - T_1) d^3}{\nu^2}$ stands for temperature Grashoff number, $Gr_C = \frac{g\beta_C (C_2 - C_1) d^3}{\nu^2}$ stands for mass Grashoff number, $\beta = \frac{Gr_C}{Gr_T}$ is the buoyancy ratio, $\lambda = \frac{Gr_T}{\mathrm{Re}}$ is the mixed convection parameter, $M^2 = \frac{\sigma B_0^2 d^2}{\mu}$ indicates magnetic parameter, $K_p = \frac{d^2}{\kappa}$ implies porosity parameter, $\mathrm{Pr} = \frac{\mu C_p}{K_f}$ signifies Prandtl number, $Ec = \frac{u_0^2}{C_p (T_2 - T_1)}$ symbolizes Eckert number, $D_f = \frac{DK_T (C_2 - C_1)}{\nu C_s C_p (T_2 - T_1)}$ is for Dufour number, $Sc = \frac{\nu}{D}$ displays Schmidt number, $Sr = \frac{DK_T (T_2 - T_1)}{\nu T_m (C_2 - C_1)}$ shows thermo-diffusion or Soret parameter, $K = \frac{K_1 d^2}{\nu}$ represents chemical reaction parameter, $\beta_1 = \frac{\gamma_1}{d}$ and $\beta_2 = \frac{\gamma_2}{d}$ illustrates the slip parameters. At the vertical wall the skin friction coefficients (C_f), Nusselt number (Nu) and Sherwood number (Sh) are given by:

$$\begin{aligned} \mathrm{Re}\,C_{f_1} &= f'(-1), \ \mathrm{Re}\,C_{f_2} = f'(1); \\ Nu_{1,2} &= -\theta'(\eta)|_{\eta=-1,1}, \\ Sh_{1,2} &= -\varphi'(\eta)|_{\eta=-1,1}, \end{aligned} \tag{2.11}$$

where

$$\begin{aligned} C_f &= \frac{\tau_w}{\rho u_0^2}, \ Nu = \frac{q_w d}{K_f (T_2 - T_1)}, \\ Sh &= \frac{q_m d}{D (C_2 - C_1)}; \end{aligned} \tag{2.12}$$

and

$$\begin{aligned} \tau_w &= \mu\frac{\partial u}{\partial y}\bigg|_{y=\pm d}, \ q_w = -K_f\frac{\partial T}{\partial y}\bigg|_{y=\pm d}, \\ q_m &= -D\frac{\partial C}{\partial y}\bigg|_{y=\pm d}. \end{aligned} \tag{2.13}$$

3. Methodology

For the OHAM calculation, we guess an accurate analytical approximation of ve-

locity $f(\eta)$, temperature $\theta(\eta)$, and mass $\varphi(\eta)$ satisfying boundary condition equation (2.10) as follows:

$$f_0(\eta) = 0,\ \theta_0(\eta) = \frac{1+\eta}{2},\ \varphi_0(\eta) = \frac{1+\eta}{2}; \tag{3.1}$$

and the auxiliary linear operators for velocity, temperature and mass profiles are

$$L_f = \frac{\partial^2}{\partial\eta^2},\ L_\theta = \frac{\partial^2}{\partial\eta^2},\ L_\varphi = \frac{\partial^2}{\partial\eta^2}. \tag{3.2}$$

Introducing zeroth-order deformations as

$$\begin{aligned}&(1-p)\,L_f\left[f(\eta;p) - f_0(\eta)\right]\\ &= ph_f N_f\left[f(\eta;p), \theta(\eta;p), \varphi(\eta;p)\right];\end{aligned} \tag{3.3}$$

$$\begin{aligned}&(1-p)\,L_\theta\left[\theta(\eta;p) - \theta_0(\eta)\right]\\ &= ph_\theta N_\theta\left[f(\eta;p), \theta(\eta;p), \varphi(\eta;p)\right];\end{aligned} \tag{3.4}$$

$$\begin{aligned}&(1-p)\,L_\varphi\left[\varphi(\eta;p) - \varphi_0(\eta)\right]\\ &= ph_\varphi N_\varphi\left[\theta(\eta;p), \varphi(\eta;p)\right];\end{aligned} \tag{3.5}$$

subject to the boundary conditions

$$\begin{aligned}&f(-1;p) - \beta_1 f'(-1;p) = 0,\ \theta(-1;p) = 0,\\ &\varphi(-1;p) = 0,\ f(1;p) - \beta_2 f'(1;p) = 0,\\ &\theta(1;p) = 1,\ \varphi(1;p) = 1,\end{aligned} \tag{3.6}$$

where $p \in [0,1]$ is the embedding parameter, h_f, h_θ, and h_φ indicate non-zero auxiliary parameters, N_f, N_θ, and N_φ are the nonlinear operators denoted as:

$$\begin{aligned}&N_f\left[f(\eta;p), \theta(\eta;p), \varphi(\eta;p)\right]\\ &= \frac{\partial^2 f(\eta;p)}{\partial\eta^2} - R\frac{\partial f(\eta;p)}{\partial\eta}\\ &\quad + \lambda\left(\theta(\eta;p) + \beta\varphi(\eta;p)\right)\\ &\quad - \left(M^2 + K_p\right) f(\eta;p);\end{aligned} \tag{3.7}$$

$$\begin{aligned}&N_\theta\left[f(\eta;p), \theta(\eta;p), \varphi(\eta;p)\right]\\ &= \frac{\partial^2\theta(\eta;p)}{\partial\eta^2} - R\,\mathrm{Pr}\,\frac{\partial\theta(\eta;p)}{\partial\eta}\\ &\quad + \mathrm{Pr}\,Ec\left(\frac{\partial f(\eta;p)}{\partial\eta}\right)^2 + \mathrm{Pr}\,D_f\frac{\partial^2\varphi(\eta;p)}{\partial\eta^2}\\ &\quad + \mathrm{Pr}\,EcK_p(f(\eta;p))^2;\end{aligned} \tag{3.8}$$

$$\begin{aligned}&N_\varphi\left[\theta(\eta;p), \varphi(\eta;p)\right]\\ &= \frac{\partial^2\varphi(\eta;p)}{\partial\eta^2} - RSc\frac{\partial\varphi(\eta;p)}{\partial\eta}\\ &\quad + ScSr\frac{\partial^2\theta(\eta;p)}{\partial\eta^2} - KSc\varphi(\eta;p).\end{aligned} \tag{3.9}$$

The m^{th}-order deformation equations are given as

$$L_f\left[f_m(\eta) - \chi_m f_{m-1}(\eta)\right] = h_f R_m^f(\eta); \tag{3.10}$$

$$L_\theta\left[\theta_m(\eta) - \chi_m\theta_{m-1}(\eta)\right] = h_\theta R_m^\theta(\eta); \tag{3.11}$$

$$L_\varphi\left[\varphi_m(\eta) - \chi_m\varphi_{m-1}(\eta)\right] = h_\varphi R_m^\varphi(\eta); \tag{3.12}$$

and boundary conditions are

$$\begin{aligned}&f_m(-1) = 0, \theta_m(-1) = 0, \varphi_m(-1) = 0,\\ &f_m(1) = 0, \theta_m(1) = 0, \varphi_m(1) = 0.\end{aligned} \tag{3.13}$$

The nonlinear operators are defined as

$$\begin{aligned}R_m^f(\eta) =& f''_{m-1} - Rf'_{m-1} + \lambda\left(\theta_{m-1} + \beta\varphi_{m-1}\right)\\ &- \left(M^2 + K_p\right) f_{m-1};\end{aligned} \tag{3.14}$$

$$\begin{aligned}R_m^\theta(\eta) =& \theta''_{m-1} - R\,\mathrm{Pr}\,\theta'_{m-1}\\ &+ \mathrm{Pr}\,Ec\sum_{n=0}^{m-1} f'_{m-1-n}f'_n + \mathrm{Pr}\,D_f\varphi''_{m-1}\\ &+ \mathrm{Pr}\,EcK_p\sum_{n=0}^{m-1} f_{m-1-n}f_n;\end{aligned} \tag{3.15}$$

$$R_m^{\varphi}(\eta) = \varphi''_{m-1} - RSc\varphi'_{m-1} + ScSr\theta''_{m-1} - KSc\varphi_{m-1}; \quad (3.16)$$

In which

$$\chi_m = \begin{cases} 0, & m \le 1, \\ 1, & m > 1. \end{cases} \quad (3.17)$$

For $p = 0$ and $p = 1$, we have

$$\begin{aligned} &f(\eta;0) = f_0(\eta),\ \theta(\eta;0) = \theta_0(\eta), \\ &\varphi(\eta;0) = \varphi_0(\eta), \\ &f(\eta;1) = f(\eta),\ \theta(\eta;1) = \theta(\eta), \\ &\varphi(\eta;1) = \varphi(\eta). \end{aligned} \quad (3.18)$$

We have to assume the initial guess approximations $f_0(\eta)$, $\theta_0(\eta)$, and $\varphi_0(\eta)$, the auxiliary parameters h_f, h_θ, and h_φ, and the linear operators L_f, L_θ, and L_φ to be selected such that at every point $p \in [0,1]$ equations (3.3) - (3.5) have a solution. By using Taylor's series and equation (3.18); $f(\eta;p)$, $\theta(\eta;p)$, and $\varphi(\eta;p)$ can be presented as

$$f(\eta;p) = f_0(\eta) + \sum_{m=1}^{\infty} f_m(\eta)p^m; \quad (3.19)$$

$$\theta(\eta;p) = \theta_0(\eta) + \sum_{m=1}^{\infty} \theta_m(\eta)p^m; \quad (3.20)$$

$$\varphi(\eta;p) = \varphi_0(\eta) + \sum_{m=1}^{\infty} \varphi_m(\eta)p^m. \quad (3.21)$$

It is also assumed that the m^{th}-order derivative of $f(\eta)$, $\theta(\eta)$, and $\varphi(\eta)$ with respect to p exist and are given by

$$f_m(\eta) = \frac{1}{m!}\frac{\partial^m f(\eta;p)}{\partial p^m}\bigg|_{p=0}; \quad (3.22)$$

$$\theta_m(\eta) = \frac{1}{m!}\frac{\partial^m \theta(\eta;p)}{\partial p^m}\bigg|_{p=0}; \quad (3.23)$$

$$\varphi_m(\eta) = \frac{1}{m!}\frac{\partial^m \varphi(\eta;p)}{\partial p^m}\bigg|_{p=0}. \quad (3.24)$$

The auxiliary parameters are chosen properly such that the series (3.22) - (3.24) are convergent at $p = 1$. Therefore, by putting Eq. (3.18) into (3.22)-(3.24) at $p = 1$ we get

$$f(\eta) = f_0(\eta) + \sum_{m=1}^{\infty} f_m(\eta); \quad (3.25)$$

$$\theta(\eta) = \theta_0(\eta) + \sum_{m=1}^{\infty} \theta_m(\eta); \quad (3.26)$$

$$\varphi(\eta) = \varphi_0(\eta) + \sum_{m=1}^{\infty} \varphi_m(\eta). \quad (3.27)$$

Now, the basic solution of Eqs. (3.10)-(3.12) can be written as

$$f_m(\eta) = f_m^*(\eta) + c_1 + c_2\eta; \quad (3.28)$$

$$\theta_m(\eta) = \theta_m^*(\eta) + c_3 + c_4\eta; \quad (3.29)$$

$$\varphi_m(\eta) = \varphi_m^*(\eta) + c_5 + c_6\eta. \quad (3.30)$$

Here $f_m^*(\eta)$, $\theta_m^*(\eta)$ and $\varphi_m^*(\eta)$ are special solutions.

4. Results and Discussions

We analyzed the influence of various parameters that arise in the study of velocity, temperature, and concentration distributions. The OHAM technique was applied for the numerical solution of ordinary differential equations. The solutions are obtained graphically and the presence of these parameters on physical quantities is shown through tables. The profiles of velocity $f(\eta)$, temperature $\theta(\eta)$, and concentration $\varphi(\eta)$ are calculated and displayed via plots in Fig. 2 to 10 with dissimilar values of β_1, β_2, M, K_p, D_f, K and Sr when the other parameters are at uniform value. By using OHAM, numerical values of average square residual errors are calculated at different orders and indicated in Table 1. Values of optimal convergence control parameter at various orders of estimations are shown in Table 2. The convergence of obtained series

solution is presented in Table 3. The effect of distinct values of various parameters β_1, β_2, M, K_p, D_f, K and Sr on skin friction coefficient, Nusselt number and Sherwood number are analyzed and displayed in Table 4. Fig. 2 represents the effect of slip flow variable β_1 on $f(\eta)$. It is observed from the figure that expansion in the slip flow parameter, increases fluid velocity $f(\eta)$ because the slip parameter reduces the frictional forces between the fluid layers and, as a result, fluid velocity increases. Varying the value of slip flow variable β_2 on $f(\eta)$ can be observed in Fig. 3. It is clearly shown that with an increment in slip parameter β_2, fluid velocity decreases and slip velocity increases. The effect of the magnetic parameter on fluid velocity can be seen in Fig. 4. It shows that the flow velocity decreases with enhancement in the magnetic parameter because in the fluid, the availability of the magnetic field induces Lorentz force, which exerts a retarding force on the fluid velocity. This force causes a dragging effect on the flow, hence the velocity decreases. This retarding force can control the fluid's velocity which is very important in MHD power generators and electromagnetic coating of materials. Fig. 5 shows the effect of increasing the value of the porosity parameter on velocity distribution. It is noticed that the velocity profile decreases with the increase of the porosity parameter because the presence of the porosity parameter offers higher restriction to the fluid flow.

Fig. 6 illustrates the influence of Dufour number on the temperature profile. An increment in Dufour number increases the thermal boundary layer thickness and the temperature distribution. A higher concentration gradient occurs due to larger values of Dufour number. Energy transfer takes place at a higher rate and, therefore, the temperature increases. The influence of Dufour number on the concentration profile is seem in Fig. 7. It is evident that concentration decreases with a rise in Dufour number. The temperature difference between the fluid and the wall decreases with an increment in Dufour number, causing more heat to be transferred to the fluid which affects the fluid's viscosity. Hence, the concentration profile decreases.

Fig. 8 illustrates the influence of various values of the chemical reaction parameter on the concentration distribution. It indicates that an enhancement in the value of the chemical reaction parameter causes a decrement in the concentration of the fluid because of a fall in chemical molecular diffusivity.

The variation of the Soret number on temperature profile is depicted in Fig. 9. The temperature and thermal boundary layer thickness decrease as the Soret number increases. The thermal diffusion of the material decreases when the Soret number increases and, thus, the temperature decreases. The effect of the Soret number on concentration is analyzed in Fig. 10. Here the concentration of the fluid rises for growing values of Soret number. In the Soret phenomenon, temperature gradient affected the concentration distribution. So, higher values of the Soret number result in higher convective flow and, hence, concentration increases.

Table 1 shows the values of average square residual error up to 30^{th} order for velocity, temperature and mass profiles. It is noticed that the errors are continuously decreasing as we increase the order. Table 2 represents the optimal convergence control parameter of various orders.

Table 3 shows that for a convergent solution, the 40^{th} order of approximations is sufficient for the analysis under consideration. It gives velocity, temperature and

mass profiles at $\eta = 0$.

Table 4 explores the effects of various dimensionless parameters, such as velocity slip parameter, magnetic parameter, porosity parameter, Dufour number, Soret number and chemical reaction parameter on skin friction coefficient, Nusselt number and Sherwood number at injection and suction walls in the channel.

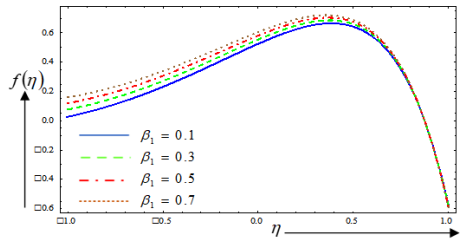

Fig. 2. Variation in $f(\eta)$ with β_1.

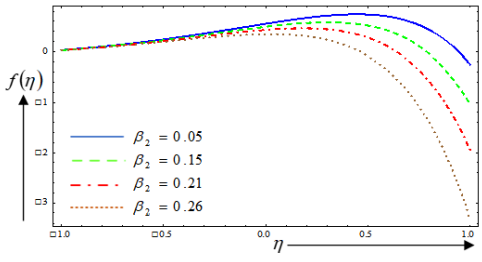

Fig. 3. Variation in $f(\eta)$ with β_2.

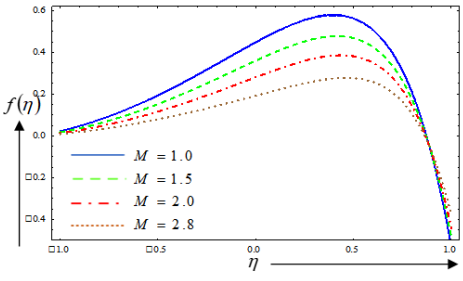

Fig. 4. Variation in $f(\eta)$ with M.

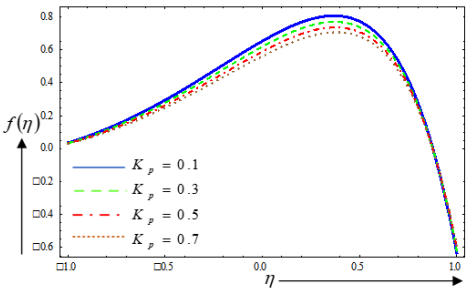

Fig. 5. Variation in $f(\eta)$ with K_p.

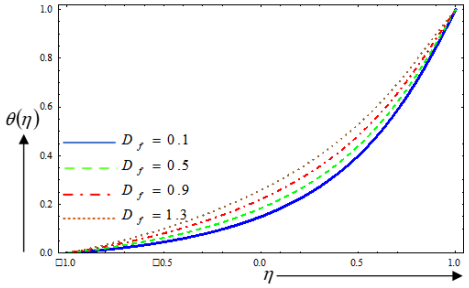

Fig. 6. Variation in $\theta(\eta)$ with D_f.

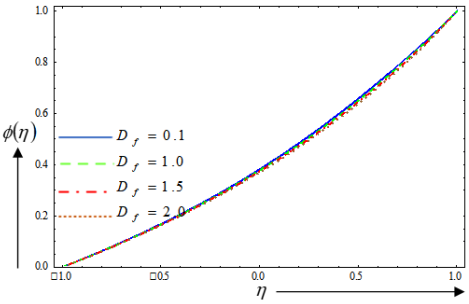

Fig. 7. Variation in $\varphi(\eta)$ with D_f.

5. Conclusions

The relevant findings are summarized as:

- Flow velocity rises due to increment in slip parameter β_1, while an increment in β_2 causes the flow velocity to reduce.

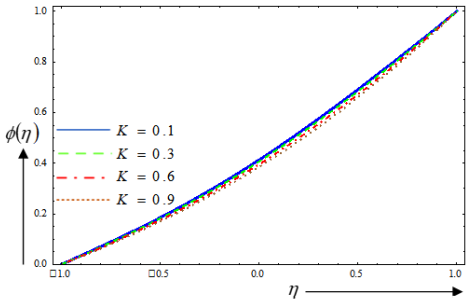

Fig. 8. Variation in $\varphi(\eta)$ with K.

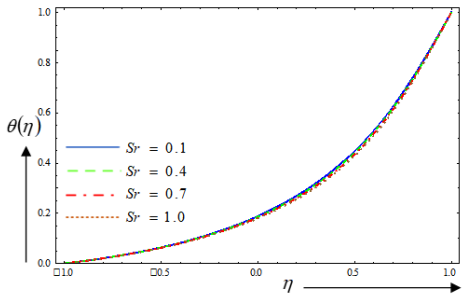

Fig. 9. Variation in $\theta(\eta)$ with Sr.

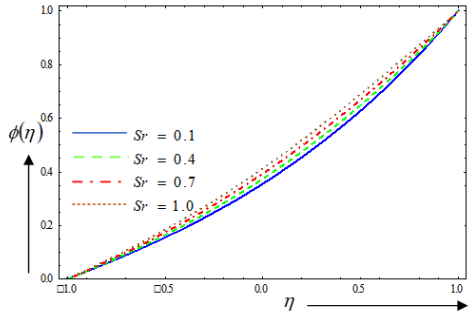

Fig. 10. Variation in $\varphi(\eta)$ with Sr.

- The fluid velocity drops as we increase the intensity of the magnetic parameter and porosity parameter.
- Temperature increases while the concentration profile decreases as Dufour parameter increases.

Table 1. Numerical values of average square residual errors.

Order of approximations	$E_{f,m}$	$E_{\theta,m}$	$E_{\varphi,m}$
4	8.925×10^{-2}	2.242×10^{-2}	7.462×10^{-3}
8	4.165×10^{-4}	1.974×10^{-4}	6.945×10^{-5}
12	5.698×10^{-6}	1.477×10^{-6}	3.194×10^{-7}
16	5.443×10^{-8}	1.627×10^{-8}	1.545×10^{-9}
20	9.413×10^{-10}	1.761×10^{-10}	1.657×10^{-11}
24	1.207×10^{-11}	2.198×10^{-12}	1.192×10^{-13}
28	1.950×10^{-13}	2.844×10^{-14}	1.268×10^{-15}
30	3.263×10^{-14}	2.419×10^{-15}	9.029×10^{-17}

Table 2. Optimal values of h_f, h_θ, and h_φ for velocity, temperature and mass field.

Order	h_f	h_θ	h_φ	$(E_m)_{Total}$
2	-0.5723	-0.6899	-0.9831	3.4782
4	-0.6521	-0.5553	-0.4719	1.5378×10^{-1}
6	-0.7313	-0.8041	-0.7760	3.8231×10^{-3}
8	-0.7162	-0.8411	-0.5869	2.8743×10^{-4}
10	-0.6877	-0.8606	-0.8549	1.9020×10^{-5}

Table 3. Convergence of OHAM results for various order of estimates.

Order of approximations	$f(0)$	$\theta(0)$	$\varphi(0)$
5	0.54332646	0.17601286	0.38118324
10	0.50702556	0.16334275	0.38370966
15	0.50568563	0.16302570	0.38404566
20	0.50570518	0.16304248	0.38405935
30	0.50571253	0.16304535	0.38405901
40	0.50571254	0.16304536	0.38405901
50	0.50571254	0.16304536	0.38405901

- Due to the increment in chemical reaction parameter the concentration

Table 4. Effects of skin friction coefficient, Nusselt number and Sherwood number for different values of β_1, β_2, Sr, D_f, K, M and K_p .

β_1	β_2	M	K_p	D_f	Sr	K	$f'(-1)$	$f'(1)$	Nu_1^-	Nu_2^+	Sh_1^-	Sh_2^+
0.2	0.1	0.5	0.5	0.5	0.5	0.5	0.33097	-6.16883	-0.10639	-1.32746	-0.33695	-0.72324
0.3	0.1	0.5	0.5	0.5	0.5	0.5	0.32603	-6.22319	-0.11045	-1.31384	-0.34253	-0.72507
0.4	0.1	0.5	0.5	0.5	0.5	0.5	0.32062	-6.27427	-0.11432	-1.30054	-0.34788	-0.72683
0.2	0.12	0.5	0.5	0.5	0.5	0.5	0.32506	-6.58247	-0.10434	-1.24713	-0.33603	-0.73227
0.2	0.15	0.5	0.5	0.5	0.5	0.5	0.31437	-7.32518	-0.10132	-1.08517	-0.33359	-0.74978
0.2	0.18	0.5	0.5	0.5	0.5	0.5	0.30185	-8.26722	-0.09913	-0.85013	-0.33012	-0.77455
0.2	0.1	0.6	0.5	0.5	0.5	0.5	0.31903	-6.07882	-0.10320	-1.34946	-0.33469	-0.72066
0.2	0.1	0.7	0.5	0.5	0.5	0.5	0.30512	-5.97897	-0.09965	-1.37348	-0.33206	-0.71777
0.2	0.1	0.8	0.5	0.5	0.5	0.5	0.28939	-5.87163	-0.09588	1.39884	-0.32928	-0.71466
0.2	0.1	0.5	0.4	0.5	0.5	0.5	0.34102	-6.24829	-0.10781	-1.31290	-0.33737	-0.72446
0.2	0.1	0.5	0.6	0.5	0.5	0.5	0.32098	-6.09322	-0.10457	-1.34132	-0.33614	-0.72197
0.2	0.1	0.5	0.8	0.5	0.5	0.5	0.30110	-5.95211	-0.10011	-1.36729	-0.33347	-0.71915
0.2	0.1	0.5	0.5	0.1	0.5	0.5	0.31594	-6.02845	-0.06749	-1.49322	-0.37550	-0.71603
0.2	0.1	0.5	0.5	0.4	0.5	0.5	0.32997	-6.13273	-0.09933	-1.37058	-0.34482	-0.72063
0.2	0.1	0.5	0.5	0.7	0.5	0.5	0.33164	-6.24456	-0.11877	-1.23799	-0.32753	-0.73119
0.2	0.1	0.5	0.5	0.5	0.1	0.5	0.32228	-6.08080	-0.12964	1.30077	-0.37755	-0.81998
0.2	0.1	0.5	0.5	0.5	0.2	0.5	0.32655	6.10197	-0.12112	-1.30669	-0.35750	-0.79453
0.2	0.1	0.5	0.5	0.5	0.3	0.5	0.32905	-6.12363	-0.11475	-1.31320	-0.34541	-0.77010
0.2	0.1	0.5	0.5	0.5	0.5	0.1	0.35481	-6.24170	-0.11828	-1.34743	-0.37945	-0.66193
0.2	0.1	0.5	0.5	0.5	0.5	0.3	0.34187	-6.20420	-0.11128	-1.33756	-0.35530	-0.69309
0.2	0.1	0.5	0.5	0.5	0.5	0.6	0.32615	-6.15184	-0.10453	-1.32236	-0.32932	-0.73800

profile decreases.

- The concentration of the fluid grows and temperature declines for a rise in the Soret parameter.

Nomenclature

B_0 magnetic field $(A\,m^{-1})$
C mass concentration $(mol\,m^{-3})$
C_f skin friction coefficient
C_p specific heat
C_s concentration susceptibility
C_1, C_2 mass of both plates $(mol\,m^{-3})$
D mass diffusivity $(m^2\,s^{-1})$
D_f Dufour number
Ec Eckert number
f dimensionless velocity
g acceleration in behalf of gravity $(m\,s^{-2})$
K chemical reaction parameter K_f thermal diffusion $(m^2\,s^{-1})$

K_p porosity parameter
K_T thermal diffusion ratio
K_1 rate of chemical reaction
M magnetic parameter
Nu Nusselt number
Pr Prandtl number
q_m surface mass flux
q_w surface heat flux
R suction/injection parameter
Re Reynolds number
Sc Schmidt number
Sh Sherwood number
Sr Soret number
T fluid temperature (K)
T_m mean fluid temperature (K)
T_1, T_2 temperature of both plates (K)
u velocity component in x-direction $\left(m\,s^{-1}\right)$
v velocity component in y-direction $\left(m\,s^{-1}\right)$
v_0 suction/injection velocity $\left(m\,s^{-1}\right)$

Greek Symbols

α thermal diffusivity $\left(m^2\,s^{-1}\right)$
β buoyancy ratio
β_C coefficient of solutal expansion
β_T coefficient of thermal expansion
β_1, β_2 slip parameters
γ_1, γ_2 slip coefficients
θ dimensionless temperature
κ permeability of porous medium
λ mixed convection parameter
μ viscosity coefficient $\left(kg\,m^{-1}\,s^{-1}\right)$
ρ fluid density $\left(kg\,m^{-3}\right)$
σ fluid conductivity $\left(S\,m^{-1}\right)$
τ_w shearing stress
φ dimensionless concentration

References

[1] Srinivas S, Muthuraj R. Effects of thermal radiation and space porosity on MHD mixed convection flow in a vertical channel using homotopy analysis method. Commun Nonlinear Sci 2010;15:2098-108.

[2] Raftari B, Vajravelu K. Homotopy analysis method for MHD viscoelastic fluid flow and heat transfer in a channel with a stretching wall. Commun Nonlinear Sci 2012;17:4149-62.

[3] Xinhui S, Liancun Z, Ping L, Xinxin Z, Yan Z. Flow and heat transfer of a micropolar fluid in a porous channel with expanding or contracting walls. Int J Heat Mass Transf 2013;67:885-95.

[4] Kothandapani M, Prakash J. Effects of thermal radiation and chemical reactions on peristaltic flow of a Newtonian nanofluid under inclined magnetic field in a generalized vertical channel using homotopy perturbation method. Asia-Pac J Chem Eng 2015;10:259-72.

[5] Ellahi R, Shivanian E, Abbasbandy S, Hayat T. Numerical study of magnetohydrodynamics generalized Couette flow of Eyring-Powell fluid with heat transfer and slip condition. Int J Numer Method H 2016;26:1433-45.

[6] Sharma K, Gupta S. Analytical study of MHD boundary layer flow and heat transfer towards a porous exponentially stretching sheet in presence of thermal radiation. Int J Adv Appl Math Mech 2016;4:1-10.

[7] Kumar V, Sharma K, Sharma P. Effects of radiation in MHD fluid flow through horizontal rotating channel partially filled with porous medium and entropy generation. Acta Tech 2017;62:161-78.

[8] Selvi RK, Muthuraj R. MHD oscillatory flow of a Jeffrey fluid in a vertical porous channel with viscous dissipation. Ain Shams Eng J 2018;9:2503-16.

[9] Farooq J, Mushtaq M, Munir S, Ramzan M, Chung JD, Farooq U. Slip flow through a non-uniform channel under the influence of transverse magnetic field. Sci Rep 2018;8:1-14.

[10] Kumar D, Singh J, Tanwar K, Baleanu D. A new fractional exothermic reactions model having constant heat source in porous media with power, exponential and Mittag-Leffler laws. Int J Heat Mass Transf 2019;138:1222-27.

[11] Sushila, Singh J, Shishodia YS. An efficient analytical approach for MHD viscous flow over a stretching sheet via homotopy perturbation sumudu transform method. Ain Shams Eng J 2013;4:549-55.

[12] Reddy CR, Kaladhar K, Srinivasacharya D, Pradeepa T. Influence of Soret, Hall and Joule heating effects on mixed convection flow saturated porous medium in a vertical channel by Adomian Decomposition Method. Open Eng 2016;6:10-21.

[13] Mahmoud MAA, Megahed AM. Thermal radiation effect on mixed convection heat and mass transfer of a non-Newtonian fluid over a vertical surface embedded in a porous medium in the presence of thermal diffusion and diffusion-thermo effects. J Appl Mech Tech Phys 2013;54: 90-9.

[14] Kaladhar K, Komuraiah E. Homotopy analysis for the influence of Navier slip flow in a vertical channel with cross diffusion effects. Math Sci 2017;11:219-29.

[15] Ahmed N, Bhaattacharya DJ, Barua DP. Radiation, Soret and Dufour effects in MHD channel flow bounded by a long wavy wall and a uniformly moving parallel at wall. J Appl Math Fluid Mech 2014;6:1-19.

[16] Goswami A, Singh J, Kumar D. An efficient analytical approach for fractional equal width equations describing hydromagnetic waves in cold plasma. Physica A: Stat Mech Appl 2019;524:563-75.

[17] Goswami A, Singh J, Kumar D, Gupta S. An efficient analytical technique for fractional partial differential equations occurring in ion acoustic waves in plasma. J Ocean Eng Sci 2019;4:85-99.

[18] Kumar D, Singh J, Purohit SD, Swroop R. A hybrid analytical algorithm for nonlinear fractional wave-like equations. Math Model Nat Pheno 2019;14:1-13.

[19] Singh J, Rashidi MM, Kumar D. A hybrid computational approach for Jeffery–Hamel flow in non-parallel walls. Neural Comput Appl 2017;31:2407–13.

[20] Liao SJ. Beyond perturbation: introduction to the homotopy analysis method. New York: Chapman and Hall/CRC; 2003.

[21] Liao SJ. An optimal homotopy-analysis approach for strongly nonlinear differential equations. Commun Nonlinear Sci 2010;15:2003-16.

[22] Asghar S, Abbas Z, Mushtaq M, Hayat T. Flow and heat transfer analysis in a deformable channel. J Eng Phys Thermophys 2016;89:929-41.

[23] Ellahi R. Effects of the slip boundary condition on non-Newtonian flows in a channel. Commun Nonlinear Sci 2009;14:1377-84.

[24] Ng CO. Starting flow in channels with boundary slip. Meccanica 2017;52:45-67.

[25] Sharma K, Gupta S. Homotopy analysis solution to thermal radiation effects on MHD boundary layer flow and heat transfer towards an inclined plate with convective boundary conditions. Int J Appl Comput Math 2017;3:2533-52.

[26] Terekhov VI, Ekaid AL, Yassin KF. Laminar free convection heat transfer between vertical isothermal plates. J Eng Thermophys 2016;25:509-19.

[27] Srinivasacharya D, Shafeeurrahman M. Entropy generation due to MHD mixed convection of nanofluid in a vertical channel with Joule heating and radiation effects. Int J Eng Technol 2017;9:2713-25.